



## Research Article

# Investigation of thermo-rheological properties of Fe<sub>3</sub>O<sub>4</sub>/Ethylene glycol nanofluid in a square cavity

Mohammad KAMRAN<sup>1</sup>, Adnan QAYOUM<sup>1,\*</sup>

<sup>1</sup>Department of Mechanical Engineering, National Institute of Technology Srinagar, Hazratbal, Srinagar- J&K, 190006, India

## ARTICLE INFO

### Article history

Received: 21 February 2022

Revised: 27 May 2022

Accepted: 28 May 2022

### Keywords:

Magnetic Nanofluid; Heat Transfer Enhancement; Thermal Conductivity; Rheology; Square Cavity; Natural Convection; Numerical Simulation

## ABSTRACT

Many fluids used in heat transfer and transport phenomena restrict the effectiveness of heat exchange equipment on account of their low thermal conductivity. Using nanofluids, the effectiveness of heat exchange equipment is enhanced by many folds. The use of magnetic nanofluids for heat transfer generates a prospect of regulating flow and controlling the thermal and transport properties particularly the thermal conductivity and viscosity using an externally applied magnetic field. The present study involves synthesis of oleic acid-coated magnetic nanofluids at varying concentrations of 0 to 0.643% by volume, measurement of thermal conductivity, rheological properties and corresponding numerical simulation of Nanofluid in a heated square cavity. The thermal conductivity measurement have been carried out by transient hot-wire method using KD2-pro at varying concentrations of solid phase. The results show a significant increase in thermal conductivity with increase in particle concentration. Rheological measurements show variation in viscosity with shear rate, temperature and concentration. Moreover, it has been found that at low particle loading magnetic nanofluids exhibited Newtonian behavior unlike non-Newtonian behavior at increased concentration. Numerical simulation of the magnetic nanofluid in the heated square cavity demonstrates the immense potential of augmentation of heat transfer coefficient using such fluids.

**Cite this article as:** Kamran M, Qayoum A. Investigation of thermo-rheological properties of Fe<sub>3</sub>O<sub>4</sub>/Ethylene glycol nanofluid in a square cavity. J Ther Eng 2023;9(5):1324–1338.

## INTRODUCTION

For heat transfer applications a higher value of thermal conductivity is desirable. Most of the liquids have a low value of thermal conductivity in comparison with solids. With the incorporation of solid particles in liquids, there is an increase in thermal conductivity of the suspension [1]. But due to the large size of these micro-sized particles

(usually having high densities) these suspended particles have a tendency to settle. This problem is overcome by incorporating nanometer sized materials. Nanofluids are high performance thermal fluids synthesized by immersing nanometer-sized particles of different shapes in conventional base fluids. The high thermal conductivity augmentation obtained by adding nanoparticles to a base fluid was first reported by Masuda et al. [2] in 1993. Since

### \*Corresponding author.

\*E-mail address: [adnan@nitsri.ac.in](mailto:adnan@nitsri.ac.in)

This paper was recommended for publication in revised form by Assigned Editor Mustafa Kılıç



then there has been enormous research in the direction of nanofluids. Eastman et al. [3] synthesized copper/ethylene glycol nanofluid and observed 40% enhancement at 0.3% concentration. Choi et al. [4] observed 160% thermal conductivity enhancement for Carbon Nanotubes (CNT) dispersed in engine oil. Das et al. [5] observed a maximum of 29% thermal conductivity enhancement for 1.0% Copper oxide /water nanofluid in the temperature ranging from 21 °C to 51 °C. Hwang et al. [6] found thermal conductivity enhancement of 11.3% for MWCNT/water. Apart from single solid particles dispersed in the base fluids, research has been carried using composite or hybrid materials for thermal conductivity enhancement. Hybrid nanofluids are bi-particle or multi-particle dispersions of nanoparticles in base fluid instead of mono-nanoparticles. Hybrid nanofluids allow greater control over the properties of the nanofluid. The effect on the optical, rheological, thermal and mechanical properties of the base fluid by dispersing hybrid nanoparticles has been extensively investigated. Gulzar et al. [7] synthesized hybrid  $\text{Al}_2\text{O}_3$ - $\text{TiO}_2$  nanofluids based on Therminol-55 oil and observed that the increase in concentration of nanoparticles increased heat gain. Pourrajab et al. [8] studied combined effect of MWCNTs-COOH and silver nanoparticle and obtained thermal conductivity enhancement of 47.3% for 0.04 % silver nanoparticles and 0.16% MWCNTs compared to that of the base fluid.

Most of the studies on thermal conductivity enhancement using nanofluids include the use of non-magnetic materials but the interest in the use of magnetic nanofluids stems from the possibility of controlling the flow and thermal properties under the influence of external magnetic field. Yu et al. [9] studied the thermal conductivity of  $\text{Fe}_3\text{O}_4$ /kerosene nanofluids and reported an increase of 34%. It was reported that the nanoparticles formed chained structures in the direction of the external magnetic field. Nkurikiyimfura et al. [10] used  $\text{Fe}_3\text{O}_4$ /engine oil nanofluids in presence of magnetic field and observed increase in the thermal conductivity, the role of particle size, volume concentration, and the strength of magnetic field has been reported. Li et al. [11] also studied the effect of particle concentration, magnetic field strength and its direction on the thermal conductivity of water-based magnetic nanofluids. Parekh and Lee [12] studied  $\text{Fe}_3\text{O}_4$ /kerosene nanofluids and measured thermal conductivity variation in the temperature range of 25 °C to 65 °C. They observed a 30% enhancement in thermal conductivity. Philip et al. [13] investigated  $\text{Fe}_3\text{O}_4$ /kerosene nanofluids and observed 300% enhancement in thermal conductivity at 6.3% volume concentration in presence of external magnetic field compared to an enhancement of 23% at 7.8% volume concentration without magnetic field. Gavili et al. [14] investigated  $\text{Fe}_3\text{O}_4$ /water magnetic nanofluids with a particle size of 10nm and observed 200% thermal conductivity enhancement at 5% volume percent in the presence of external magnetic nanofluids. The literature clearly shows that magnetic nanofluids

in common base fluids like water and kerosene exhibit tremendous increase in thermal conductivity.

In order to understand the rheological behavior, viscosity is considered an important property and compared to thermal conductivity not many studies have been done on rheological properties of magnetic nanofluids. Viscosity plays an important role in determining the usability of a heat transfer fluid in thermal applications involving fluid motion. Viscosity of fluid affects the pumping power required for fluid flow and as such plays an important part in the design of thermal and fluid systems. Li et al. [15] studied the rheological behaviour of SiC-ethylene glycol nanofluids in concentration range of 0.2% to 1.0% by volume and observed that the rheological behaviour can be divided into two categories based on the concentration of nanofluids. For dilute nanofluids (volume fraction less than 0.6%) the nanofluids behaved as Newtonian fluids and for concentrated nanofluids (volume fraction greater than 0.6%) the nanofluids exhibit Non-Newtonian behaviour at lower shear rates and Newtonian behaviour at higher shear rates. Chen et al. [16] observed a shear thinning non-Newtonian behavior in ethylene glycol based  $\text{TiO}_2$  nanofluids and further concluded that the shear thinning behavior of nanofluid is mainly affected by the solid particle concentration, shear rate and the viscosity of the base liquid and exhibits a characteristic shear rate. Further they classified the nanofluids based on concentration into four categories : Dilute ( $\phi < 0.6\%$ ), semi-dilute ( $\phi < 0.6\%$ ), semi-concentrated ( $\phi < 0.6\%$ ) and concentrated ( $\phi < 0.6\%$ ) and found that shear thinning non-Newtonian behavior is visible in semi-concentrated and concentrated nanofluids. Similarly, Hong et al. [17] synthesized water based magnetic nanofluids and observed Newtonian behavior for low concentration fluids and shear thinning behavior for higher concentration magnetic nanofluids. Pastoriza-Gallego, et al. [18] studied rheological behavior of  $\text{Fe}_2\text{O}_3$  ethylene glycol nanofluids and observed non-Newtonian shear thinning behavior. Ahmadi et al. [19] investigated effect of temperature and volume fraction on viscosity of water based  $\text{Fe}_3\text{O}_4$ /MWCNT nanofluids in the concentration range of 0.1% to 1.8% and in the temperature range of 25 to 50 °C and observed viscosity to be directly proportional to volume fraction and inversely proportional to temperature. It was also seen that nanofluids behaved as Newtonian fluids upto 0.8% concentration and non-Newtonian behavior above this concentration.

Phuoc et al. [20] studied effect of shear rate and concentration on  $\text{Fe}_2\text{O}_3$ -de-ionized water nanofluids and observed viscosity to increase with volume fraction increase and subsequently as Newtonian and non-Newtonian for particle volume fraction ( $\phi$ ) below and above 0.02. Anoop et al. [21] investigated viscosity of different nanofluids at varied temperature and concentration and found reduction and increase in viscosity with increase in temperature and concentration respectively. Chen et al. [22] studied multi walled carbon nanotubes dispersed in distilled water in temperature ranging from 5 °C to 65 °C. They found that viscosity

of nanofluids increase beyond concentration of 0.004 and in addition for temperature greater than 55°C there is increase in relative viscosity ratio. Sundar et al. [23] studied Fe<sub>3</sub>O<sub>4</sub>/water nanofluid at varied particle loading (ranging from 0 to 2%) and temperature (ranging from 20 to 60 °C) and confirmed Newtonian behavior for the magnetic nanofluids in this range. The investigation confirmed the viscosity trend with increase in concentration with a maximum at 2% concentration. Afrand et al. [24] reported Newtonian behavior for Magnetite-Silver/Ethylene glycol hybrid nanofluid at particle loading of 0.3% and non-Newtonian at 0.6% and 1.2% concentration. In general it has been observed that nanofluids behave as Newtonian at lower concentrations and Non-Newtonian at higher concentration. The particular value of concentration of the transition varies from one fluid to another and as such cannot be generalized.

Ethylene glycol based nanofluids of magnetite have been synthesized in the present study. Literature shows minimal studies on thermal conductivity and rheological measurements of ethylene glycol based magnetic nanofluids at low concentration. The thermal conductivity for such fluids has been measured using KD2-pro and rheological behavior has been studied using AntonPar MCR 102 rheometer. The suitability for the heat transfer application has been numerically studied by using magnetic nanofluids in a heated square cavity.

## Experimental and Numerical Simulation Details

### Materials

Magnetite nanoparticles used in the present investigation have been procured from Platonic Nanotech Pvt. Ltd, India [26]. The average particle size is in the range of 30-50nm. The specifications of magnetite nanoparticles are presented in Table 1. Ethylene glycol and Oleic acid of 99.5% purity (procured from Rankem Chemicals, USA) have been used in the investigation.

### Nanofluid Preparation

The nanofluids have been synthesized by directly mixing the procured nanoparticles in ethylene glycol. On account of magnetic nature of the nanoparticles, use of magnetic stirrer is avoided as the nanoparticles get attracted to the

magnetic bead of the stirrer. The mixing of the nanoparticles is carried in an ultrasonicator. A specific amount of the magnetite nanoparticles has been dispersed in a specific amount of base fluid to obtain different concentrations of nanofluid. The volume fraction of nanoparticles in the base fluids are given by equation (1):

$$\varphi = \frac{\frac{m_p}{\rho_p}}{\frac{m_p}{\rho_p} + \frac{m_l}{\rho_l}} \quad (1)$$

where  $m_p$  and  $m_l$  are mass of nanoparticles and base fluid and  $\rho_p$  and  $\rho_l$  are their respective densities. Six samples were prepared with varying concentrations of magnetite in ethylene glycol viz. 0.107%, 0.214%, 0.321%, 0.428%, 0.535% and 0.642% by volume.

The sonication has been carried out for 3 hours with the addition of the surfactant after 1 hour. The amount of surfactant to be used is a very important consideration as an excess amount of surfactant leads to the formation of clumps and large aggregates. Also little quantity of the surfactant does not serve the purpose. As such an optimized amount of surfactant has to be used. The amount of surfactant added depends on the volume (mass/density) of nanoparticles to be dispersed. After completion of the sonication, the samples have been analyzed for traces of any possible clumps. For characterization involving thermal conductivity and rheology, samples with least aggregates have been selected. Figure 1 shows the effect of addition of surfactant to the magnetic nanofluid. As can be observed with the use of surfactant the nanofluid remains homogeneous with lesser sedimentation or aggregation.

### X-ray diffraction (XRD) and Scanning electron microscopy (SEM) Measurements

X-ray diffraction (XRD) measurements have been carried out with a SmartLab X-Ray Diffractometer (XRD) using Cu-K-beta radiation with a scan range of 10° to 90° at a scan speed of 21.6° per minute and a step width of 0.02°. To study the morphology of nanoparticles, Scanning Electron Microscopy (SEM) of the magnetite particles has been done using Hitachi 3600 N.

### Thermal conductivity Measurement

KD2 Pro [Decagon Devices, USA] (see Figure 2) has been used for the measurement of the thermal conductivity of the nanofluids. The setup comprises of a handheld controller and sensor needle of different types which can be slipped into the test material. In this investigation single needle KS-1 sensor (Figure 2(b)) has been used for measuring the thermal conductivity of the nanofluid. The KS-1 sensor has been selected as it uses only a small amount of heat to the nanofluid thereby reducing problems induced by free convection. The setup is based on transient hot-wire method which assumes hot wire to be an ideal, infinite and

**Table 1.** Specifications of Magnetite nanoparticles [15]

Specification	Value
Molecular weight	231.5 g/mol
Average Particle Size	30-50 nm
Specific Surface Area (SSA)	40-60m <sup>2</sup> /g
Bulk Density	0.85 g/cm <sup>3</sup>
True Density	5.1 - 5.8 g/cm <sup>3</sup>
Morphology	Spherical
Color	Dark Brown

thin line heat source surrounded in a homogeneous and isotropic medium with fixed temperature. The temperature rise  $\Delta T$  at position  $r$  from the heat source and at time  $t$  is obtained from equation (2):

$$\Delta T(r, t) = \frac{q}{4\pi k} \ln \frac{4\alpha t}{\rho^2 C} \quad (2)$$

This is a dynamic technique involving measurement of temperature rise at a fixed location from the source of heat using a single needle sensor acting as a heat source [27]. By

measuring the temperature rise in the medium with respect to time the thermal conductivity of the medium is evaluated [43-49].

**Rheological Measurements**

The viscosity of the prepared nanofluids has been measured using AntonPar MCR102 rheometer using a cone and plate arrangement with a diameter of 40 mm as shown in Figure 3. The minimum gap between the rotating and stationary plate has been maintained at 0.01 mm. To determine the flow behavior and viscosity dependence

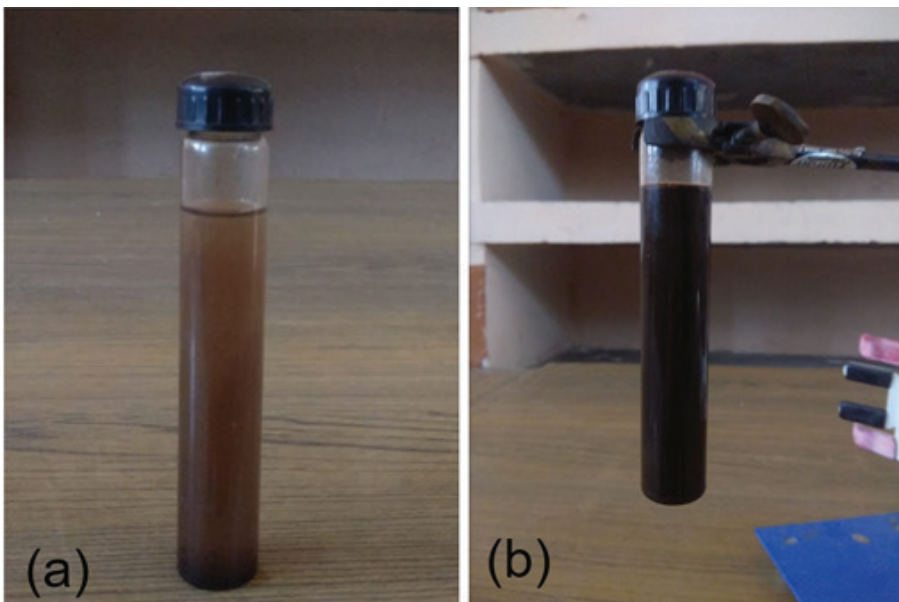


Figure 1. Effect of surfactant on the stability of nanofluid (a) without surfactant (b) With surfactant.

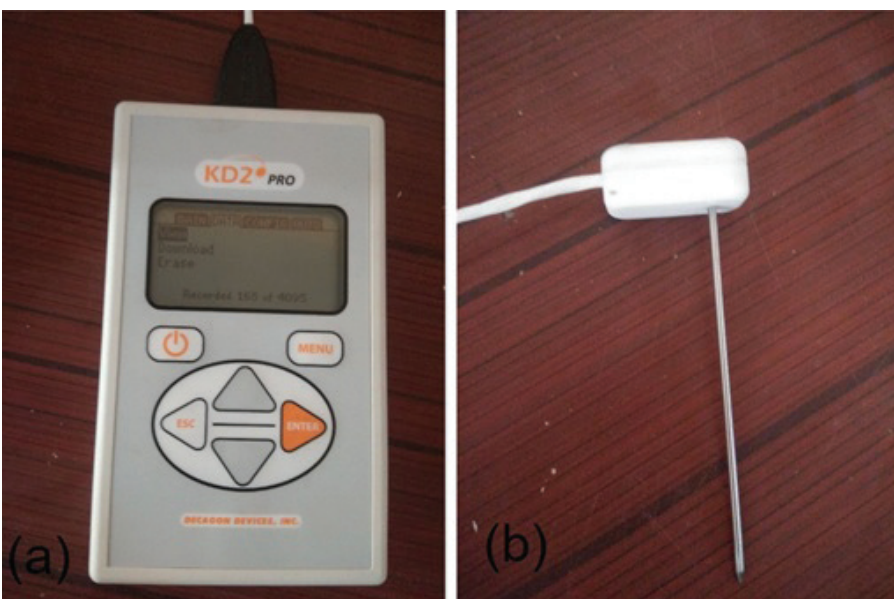
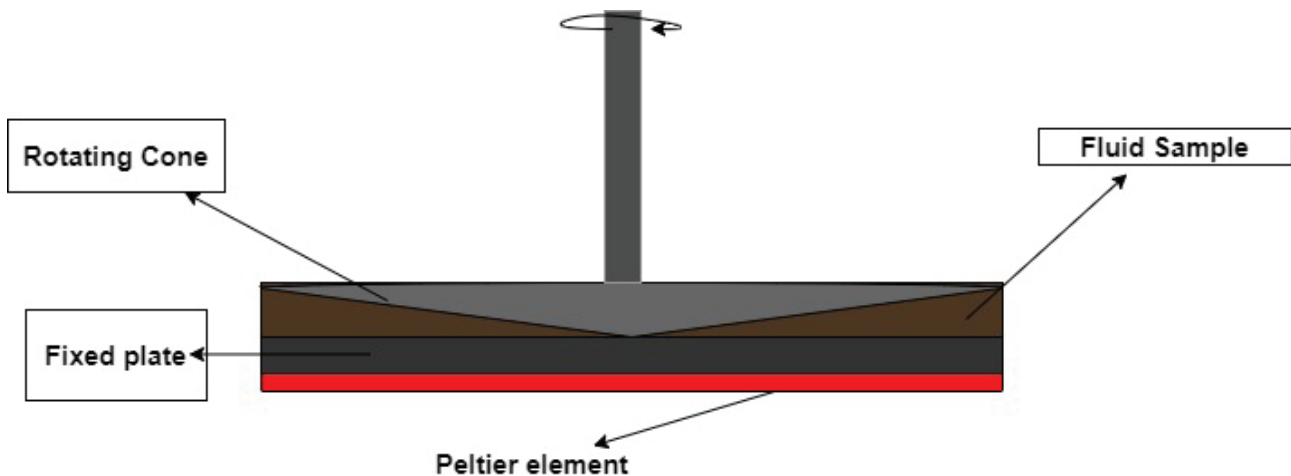


Figure 2. Thermal conductivity measurement device KD2 Pro:(a)main controller (key pad) (b)KS-1 needle sensor.



**Figure 3.** Cone and Plate system for measurement of viscosity.

on temperature, a series of experiments have been carried out at varied shear rates and temperatures in continuous rotation mode. Shear rates varying between  $100\text{s}^{-1}$  to  $500\text{s}^{-1}$  have been chosen and temperature is varied between  $20\text{ }^{\circ}\text{C}$  to  $50\text{ }^{\circ}\text{C}$ . The temperature of the system was maintained using a Peltier system (inbuilt in the rheometer) for temperature control.

#### Theoretical models of Thermal conductivity and Viscosity

Various theoretical models and empirical relations have been proposed for thermal conductivity and viscosity estimation of nanofluids. A relevant number of theoretical models for thermal conductivity are presented in Table 2, where  $k_{\text{eff}}$ ,  $k_p$  and  $k_f$  are thermal conductivities of nanofluid, nanoparticle and base fluid respectively and  $\varphi$  is the volume fraction of solid phase in the base liquid. Similarly, Table 3 presents various theoretical models and empirical relations for viscosity estimation of nanofluids.

**Table 2.** Theoretical Models for predicting Thermal conductivity of Nanofluids

Theoretical Models	Thermal conductivity enhancement ratio ( $k_{\text{eff}}/k_f$ )
Maxwell Model [28]	$\frac{k_{\text{eff}}}{k_p} = \frac{k_p + 2k_f - 2\varphi(k_f - k_p)}{k_p + 2k_f + \varphi(k_f - k_p)}$
Xue Model [29]	$1 - \varphi + 2\varphi \frac{k_p}{k_p - k_f} \ln \frac{k_p + k_f}{2k_f}$ $1 - \varphi + 2\varphi \frac{k_f}{k_p - k_f} \ln \frac{k_p + k_f}{2k_f}$
Mintsa Model [30]	$1 + 1.72\varphi$
Timofeeva Model [31]	$1 + 3\varphi$
Sundar Model [32]	$(1 + 1.05\varphi)^{0.1051}$

**Table 3.** Theoretical Models and empirical relations for Viscosity of Nanofluids

Models	Equation/Correlation
Krieger -Dougherty Model [35]	$\mu_{nf} = \mu_{bf} \left(1 - \frac{\varphi}{\varphi_m}\right)^{-\varphi_m \mu}$
Brinkman Model [36]	$\mu_{nf} = \mu_{bf} (1 - \varphi)^{-2.5}$
Batchelor Model [37]	$\mu_{nf} = \mu_{bf} (1 + 2.5\varphi + 6.5\varphi^2)$
Einstein Model [38]	$\mu_{nf} = \mu_{bf} (1 + 2.5\varphi)$
Sundar et al. [23]	$\mu_{nf} = \mu_{bf} \left(1 + \frac{\varphi}{12.5}\right)^{6.356}$
Chen et al. [16]	$\mu_{nf} = \mu_{bf} (1 + 10.6\varphi + (10.6\varphi)^2)$

#### Numerical Simulation

A numerical simulation using ANSYS Fluent has been carried for the purpose of quantifying the effect of magnetite nanoparticle in the base fluid contained in a heated square cavity. The concentration of the nanoparticle has been varied during the simulation. Although there have been many studies on free convection of different nanofluids in square cavity but all such studies have incorporated theoretical and empirical relations. In the current numerical simulation, the experimental values of thermal conductivity and viscosity obtained during characterization have been used for modeling the nanofluid in the cavity. A detailed numerical study involving fluid flow and heat transfer behavior at different values of concentrations has been presented.

#### Governing equations and problem formulation

For the simulation a differentially heated square cavity is considered, filled with  $\text{Fe}_3\text{O}_4$ / ethylene glycol nanofluid. The nanofluid is assumed to be a single phase system with thermal equilibrium between nanoparticles and base fluid and no slip in between [50-61]. The cavity has top

and bottom walls insulated with left and right walls kept at two different temperatures ( $T_h$  and  $T_c$ ) as can be seen in Figure 4(a) such that  $T_h > T_c$ . This induces natural convection heat transfer in the cavity. The nanofluid thermophysical properties at a given concentration are assumed to be fixed. Density variation with temperature is modeled using Boussinesq approximation. Moreover due to temperature difference there is buoyancy driven flow which is assumed to remain steady.

The governing equations for steady laminar flow are given by:

Continuity equation:

$$\frac{\partial(\rho_{nf}u)}{\partial y} + \frac{\partial(\rho_{nf}v)}{\partial x} = 0 \quad (3)$$

Momentum equation:

$$u \frac{\partial v}{\partial x} + v \frac{\partial v}{\partial y} = -\frac{1}{\rho_{nf}} \frac{\partial p}{\partial y} + \frac{\mu_{nf}}{\rho_{nf}} \left( \frac{\partial^2 v}{\partial x^2} + \frac{\partial^2 v}{\partial y^2} \right) + \beta_{nf} g (T - T_x) \quad (4)$$

Energy equation:

$$u \frac{\partial T}{\partial x} + v \frac{\partial T}{\partial y} = \frac{k_{nf}}{\rho_{nf} C_{p,nf}} \left( \frac{\partial^2 T}{\partial x^2} + \frac{\partial^2 T}{\partial y^2} \right) \quad (5)$$

where  $\rho_{nf}$ ,  $C_{p,nf}$ ,  $k_{nf}$ ,  $\beta_{nf}$  and  $\mu_{nf}$  are density, heat capacity, thermal conductivity, thermal expansion coefficient and viscosity of nanofluid respectively. The effect of the change in solid particle concentration on Nusselt number and heat transfer coefficient has been evaluated at different values of Rayleigh number (equation 6-9).

$$Nu = -\frac{k_{nf}}{k} \left( \frac{\partial T}{\partial x} \right) \quad (6)$$

$$Nu_{avg} = \int_0^L Nu(y) dy \quad (7)$$

$$h = \frac{q_w}{T_h - T_L} \quad (8)$$

$$Ra = \frac{g\beta\Delta TL^3}{\alpha\nu} \quad (9)$$

where  $\beta$ ,  $\alpha$  and  $\nu$  are thermal expansion coefficient, thermal diffusivity and kinematic viscosity respectively. The thermophysical properties like heat capacity, thermal expansion coefficient and density are calculated using following correlations:

$$\beta_{nf} = \varphi\beta_{np} + (1 - \varphi)\beta_{bf} \quad (10)$$

$$\rho_{nf} = \varphi\rho_{np} + (1 - \varphi)\rho_{bf} \quad (11)$$

$$C_{nf}\rho_{nf} = \varphi\rho_{np}C_{np} + (1 - \varphi)\rho_{bf}C_{bf} \quad (12)$$

where subscripts ‘bf’ refers to base fluid and ‘np’ refers to nanoparticle and  $\beta$ ,  $\rho$ ,  $C$ , and  $\varphi$  are thermal expansion coefficient, density, heat capacity and volume fraction respectively. The boundary conditions are given as :

$$\left[ \begin{array}{l} x = 0, \quad v = 0, \quad T = T_h \quad x = L, \quad v = 0, \quad T = T_c \\ y = 0, \quad v = 0, \quad \frac{\partial T}{\partial y} = 0 \quad Y = L, \quad v = 0, \quad \frac{\partial T}{\partial y} = 0 \end{array} \right] \quad (13)$$

The numerical solution of partial differential equations (3-5) along with boundary conditions (13) is obtained using commercially available finite volume method based ANSYS Fluent software. The equation (4-5) for momentum and energy are discretized using second order upwind method and SIMPLE algorithm is used for solving pressure-velocity coupling. The convergence criteria for all parameters are specified as  $10^{-6}$ .

#### Validation and Grid independency test

The present simulation is validated with the numerical results of DeVahl et al. [39] and Khanafer et al. [40] for  $Ra = 10^3$  to  $10^7$  and  $Pr = 0.7$ . The Nusselt number for present study is in good agreement with these two studies (as shown on the Table 4). In order to check the independency on mesh size four different grid sizes have been adopted (viz. 50x50, 80x80, 100x100, and 200x200). A detailed grid independency test has been done for Nusselt number at a Rayleigh number of  $10^6$ . The results are tabulated in Table 5. It is observed that with increase in fineness of mesh the percentage change in the Nusselt number is decreased. As seen from the Table 5, the percentage change in Nusselt number for mesh sizes of 80x80, 100x100 and 200x200 are 0.823%, 0.606% and 0.146% respectively with respect

**Table 4.** Code Validation

Ra	De Vahl	Khanafer	Present study
103	1.118	1.118	1.118
104	2.243	2.245	2.247
105	4.519	4.522	4.543
106	8.8	8.826	8.590

**Table 5.** Grid Independency Test

Grid size	Nusselt number	Percentage change
50x50	8.987	-
80x80	8.913	0.823%
100x100	8.859	0.606%
200x200	8.846	0.146%

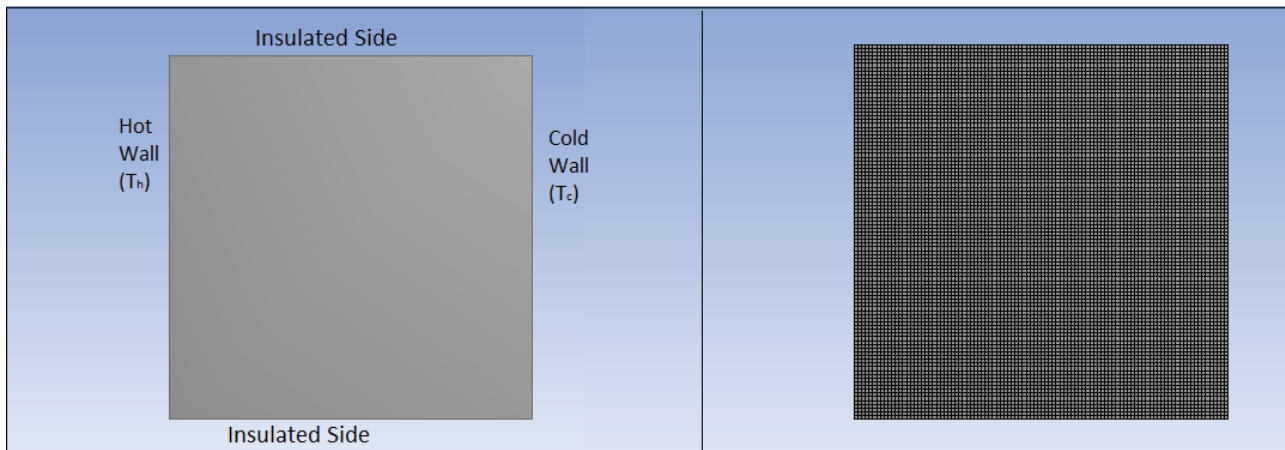


**Figure 4.** (a) Square cavity with boundary conditions (b) illustration showing 100 x 100 mesh for the square cavity.

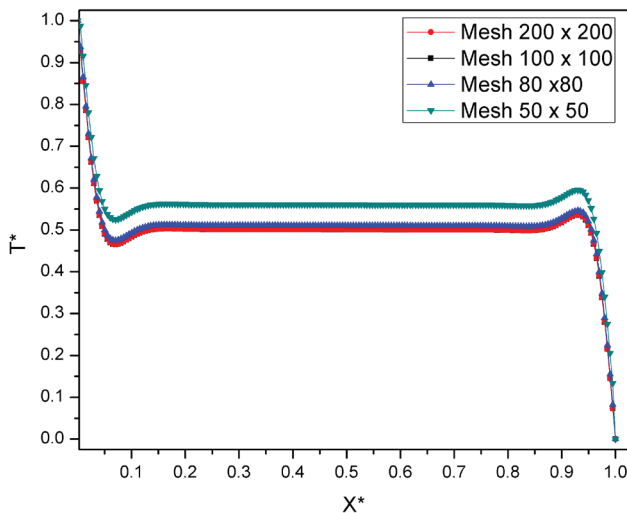


**Figure 5.** Variation of Non-dimensional temperature along x-direction at different mesh sizes (Grid independency test).

to previous mesh size. As the finer grid size solutions take more time to converge, a grid size of 100x100 is used for current simulation (see Figure 4(b)).

## RESULTS AND DISCUSSION

### XRD and SEM Results

X-ray diffraction (XRD) and scanning electron microscope (SEM) images of magnetite nanoparticles are presented in figure 6 and figure 7 respectively. The X-Ray Diffraction (XRD) results are presented in figure 6. The reflection peaks observed in the figure 5 are in agreement with the results obtainable from literature [23] and confirms face center cubic (FCC) phase of the magnetite. The analysis shows 100% crystallinity with a crystallite size of 8.2 °Å using Williamson Hall Method. Further no impurities have been observed in the sample and maximum intensity peak is observed at 35.6°

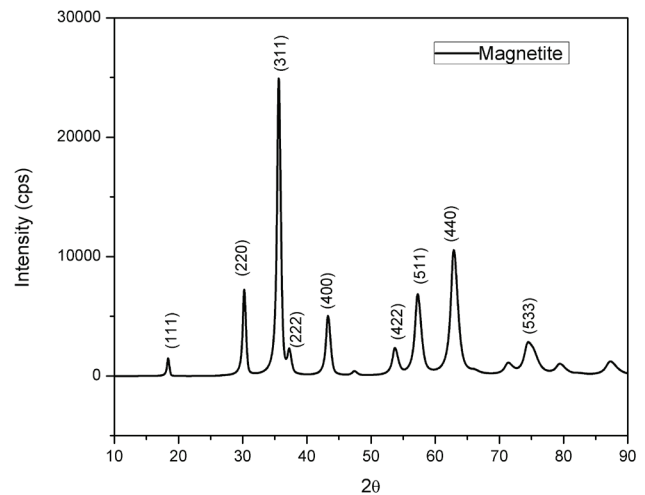


**Figure 6.** X-ray Diffraction (XRD) of Magnetite nanoparticles.

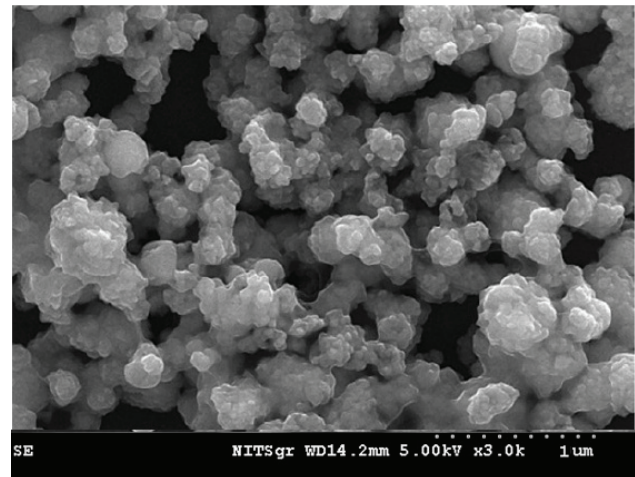


**Figure 7.** SEM image of Magnetite nanoparticles.

corresponding to index (3 1 1). SEM analysis is used to examine the morphology of nanoparticles and the results confirm that magnetite nanoparticles are spherical in shape.

### Thermal Conductivity Results

The variation of thermal conductivity has been studied with respect to the concentration of nanoparticles. It has been observed that there is increase in thermal conductivity with an increase in concentration. The results are presented in Figure 8. At a low value of concentration, there is not much increase in thermal conductivity and a maximum thermal conductivity of 0.273 W/m K is observed at 0.643% concentration for this case. Figure 9 shows variation of thermal conductivity enhancement ratio with concentration. The highest enhancement in thermal conductivity is observed to be 7% at 0.643% by volume with respect to the ethylene glycol. Figure 10 shows the comparison of the experimental values of thermal conductivity with various theoretical models. It is evident from the figure that no model is able to make a correct prediction of thermal conductivity in this case.

### Rheological Results

Figure 11 presents nanofluid flow behavior for varying shear strain rate from 100 s<sup>-1</sup> to 500 s<sup>-1</sup>. It is observed that the viscosity of ethylene glycol remains constant and follows a Newtonian behavior in agreement with the literature [18]. Newtonian behavior is also observed at low concentrations. As the concentration increases the behavior changes to Non-Newtonian on account of shear thinning behavior, as reported in literature for different nanofluids [22]. The figure clearly shows that the flow behavior is dependent on concentration of nanofluid. At low shear rates the non-Newtonian behavior is more prominent for higher concentrations and as the shear rate increases the Newtonian behavior begins to overcome the Non Newtonian behavior. This behavior of nanofluids exhibits dependency of flow behavior on the shear rate and concentration.

Figure 12 shows absolute viscosity plotted with particle loading (volume percent) at various temperatures. It is clear that viscosity decreases with temperature for all values of concentrations and increases with increase in concentration. For 0.107 % volume percent, a maxima and minima of 19.1 mPa.s and 6.6 mPa.s respectively are observed at 20 °C and 55 °C. Similarly for 0.214%, 20.86 mPa.s and 7.2 mPa.s are observed at 20 °C and 55 °C respectively . For highest concentration of 0.643%, the maxima and minima of 24.8 mPa.s and 8.4 mPa.s are observed at 20 °C and 55 °C. Figure 12 presents viscosity enhancement ( $\mu_{enh} = \frac{\mu_{nf}}{\mu_{bf}}$ ) plotted against temperature for various concentrations. Viscosity enhancement in the figure 13 is defined as ratio of viscosity of nanofluid to that of the base fluid at a given temperature. It is observed that viscosity enhancement is strongly dependent on the concentration and is not affected by temperature which is well in agreement with the results from literature [16]. An average viscosity enhancement of 8.2%, 18%, 34.4% 40.2%, is observed for 0.107%, 0.214%, 0.432% and 0.643% concentration respectively. This increase in

viscosity can be attributed to decrease in distance between particles with increase in concentration and thus leading to increased interaction between them [25].

Figure 14 shows comparison of the experimental data with the various theoretical models and empirical relations available in the literature [16, 23, 35, 36, 37, 38]. It is observed that the theoretical models cannot predict the viscosity enhancement of the nanofluids and all the values are underestimated as compared to the experimental values. The results slightly match with the results of Sundar *et al.* [23]. Figure 15 shows comparison of viscosity enhancement ratio of present study with the literature [15,19,23]. The results are in good agreement with those obtained by Xi *et al.* [15] for ethylene glycol based SiC nanofluids and Ahmadi *et al.* [19] for ethylene glycol based Fe<sub>3</sub>O<sub>4</sub>/MWCNT nanofluids. Figure 16 shows thermal conductivity enhancement ratio (in absence of magnetic field) and viscosity enhancement ratio for magnetic nanofluids plotted with respect to concentration at 25 °C. It is clear that the enhancement in viscosity is much more for ethylene glycol based Fe<sub>3</sub>O<sub>4</sub> nanofluids compared to enhancement in thermal conductivity. Figure 17 presents combined effect of enhancement in thermal conductivity and viscosity. A factor E(K/V) is defined for this purpose as :

$$E(K/V) = \frac{\frac{\Delta k}{k}}{\frac{\Delta \mu}{\mu}} \tag{3}$$

where  $\Delta k$  and  $\Delta \mu$  are the enhancements in thermal conductivity and viscosity respectively and  $\mu$  and  $k$  are the viscosity and thermal conductivity of the base fluid respectively. It is observed that the value of E(K/V) is always less than 1 and as the concentration increases, there is a decrease in this ratio. This implies a larger pumping power compared to heat transfer augmentation.

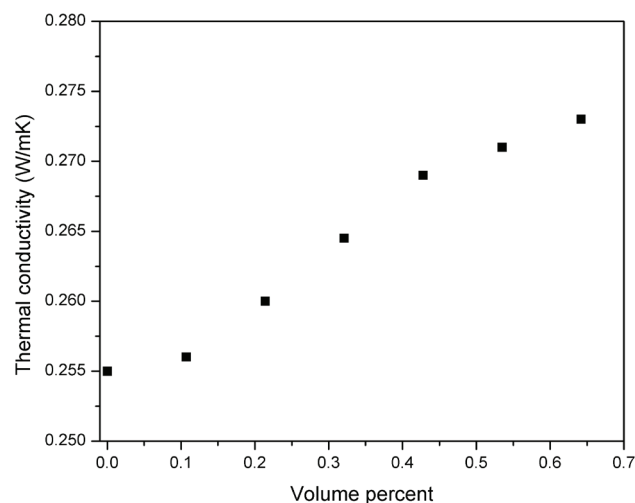


Figure 8. Variation of Thermal conductivity of Magnetic Nanofluid with volume fraction.

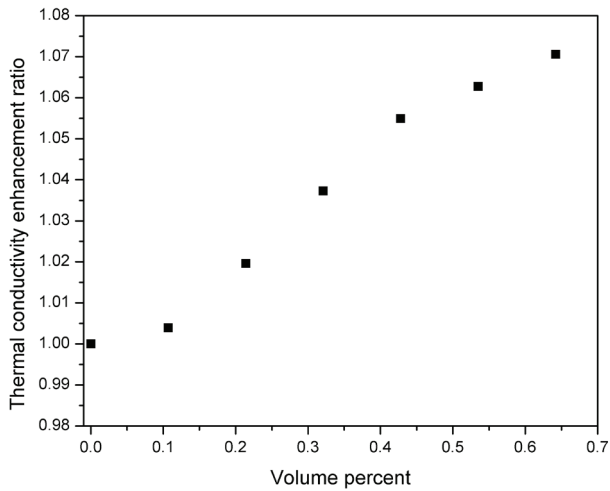


Figure 9. Variation of Thermal conductivity enhancement ratio with volume percent.

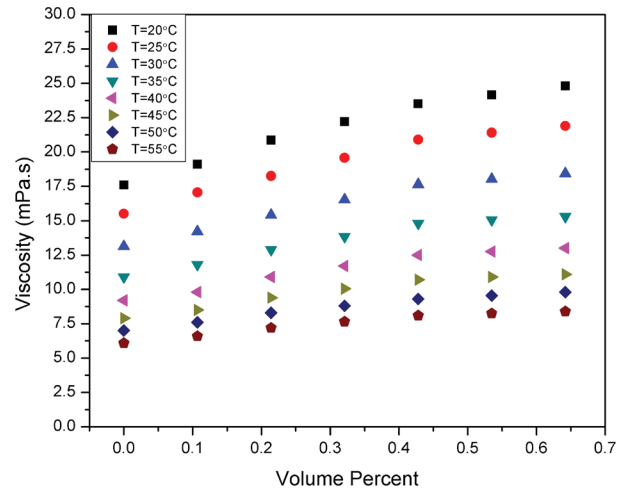


Figure 12. Variation of absolute viscosity with volume percent at varied temperatures.

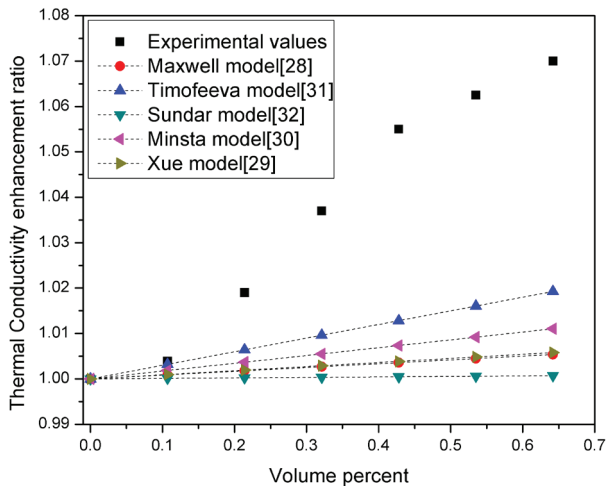


Figure 10. Comparison between Theoretical and Experimental values of Thermal conductivity of Magnetic Nanofluid at various concentrations.

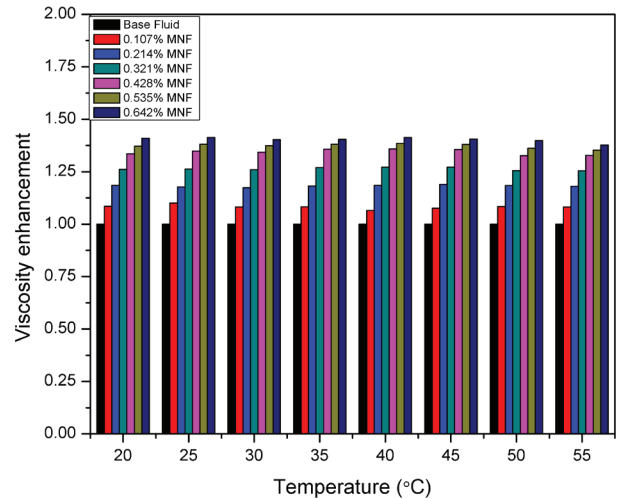


Figure 13. Comparison of Viscosity enhancement ratio for various concentrations at different temperatures.

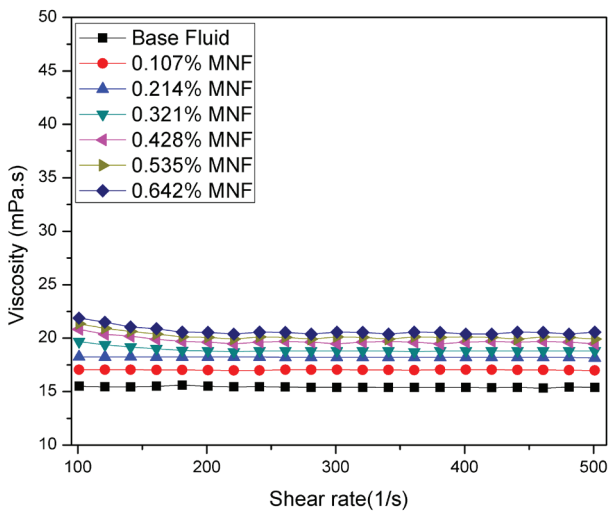


Figure 11. Flow behavior of magnetic nanofluid at various concentrations.

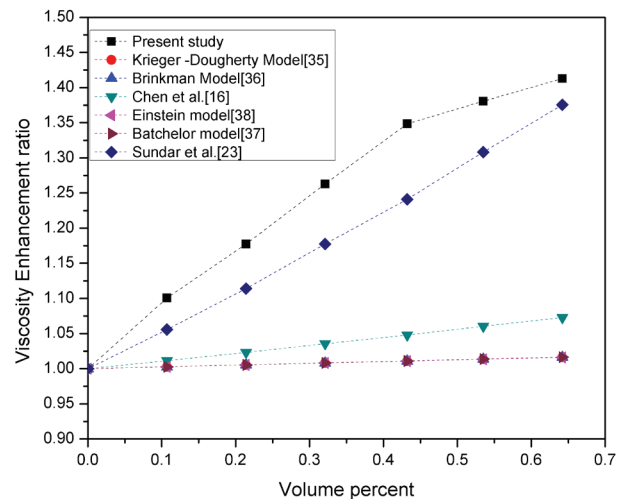


Figure 14. Comparison of viscosity enhancement ratio with theoretical models and empirical relations.

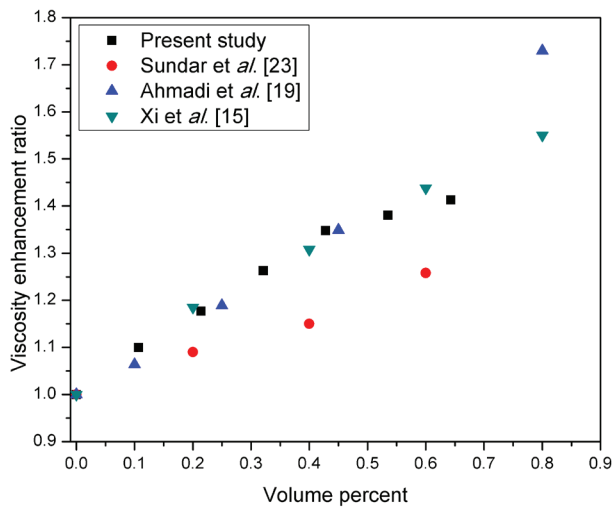


Figure 15. Comparison viscosity enhancement for present study with data available from literature.

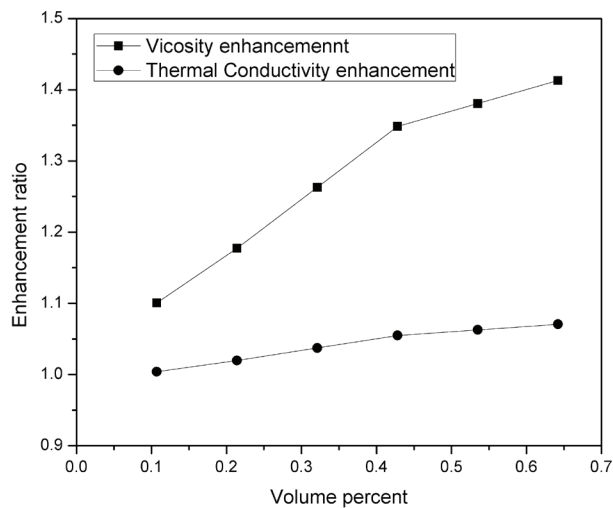


Figure 16. Comparison of thermal conductivity enhancement ratio and viscosity enhancement ratio with concentration.

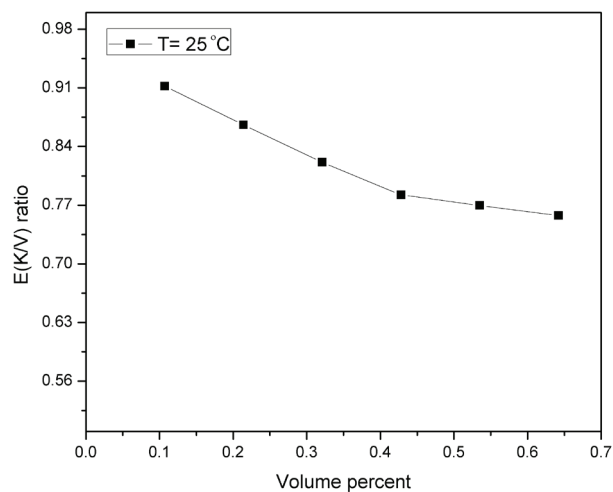


Figure 17. Variation of the ratio of enhancement of thermal conductivity and viscosity with concentration.

### Numerical Simulation Results

Numerical study of buoyancy driven free convection in a distinctly heated square cavity has been performed using experimental values of thermal conductivity and viscosity of the nanofluids. The effect of concentration and Rayleigh number on the fluid flow and heat transfer characteristics is examined. It is observed that with rise in concentration and Rayleigh number intensity of heat transfer by natural convection increases. Since a maximum concentration of 0.243% is analyzed the effect of Rayleigh number is more pronounced than that of concentration. Figure 18 and figure 19 presents enhancement of heat transfer coefficient and Nusselt number respectively. It is observed that Nusselt number and heat transfer coefficient are strongly influenced by the Rayleigh number. For 0.107% concentration

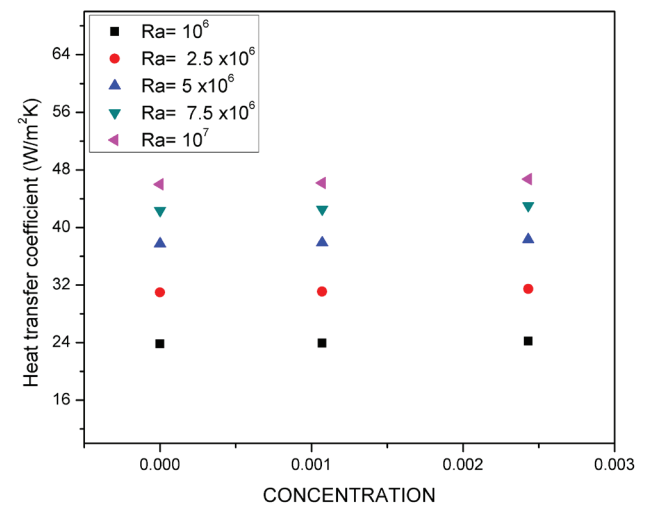


Figure 18. Variation of Heat transfer coefficient (h) with concentration for Rayleigh number in range  $10^6$  to  $10^7$ .

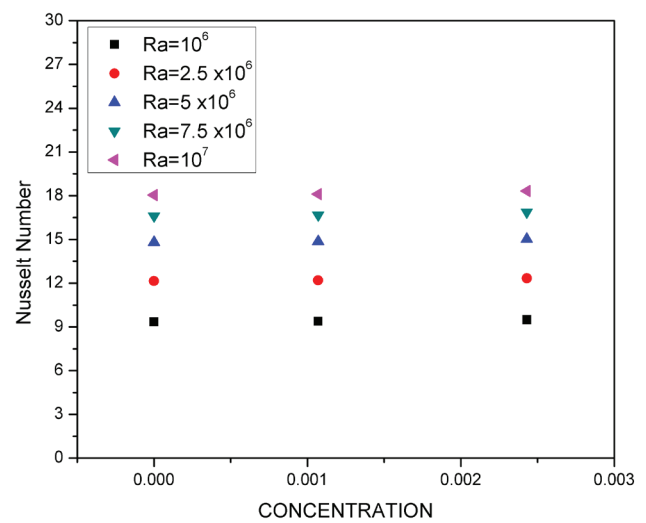
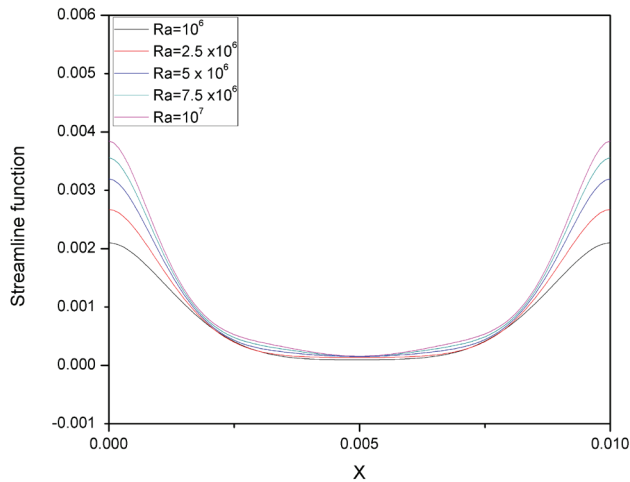


Figure 19. Variation of Nusselt Number (Nu) with concentration for Rayleigh number in range  $10^6$  to  $10^7$ .



an enhancement of 0.38% to 0.39% is observed for Nusselt number and heat transfer coefficient at all values of Rayleigh number in comparison to the base fluid. For 0.243% concentration the enhancement in heat transfer coefficient and Nusselt number is found to be 1.56% with respect to base fluid. Also as the Rayleigh number increases from  $10^6$  to  $10^7$  there is nearly 93% enhancement in heat transfer coefficient and Nusselt number. Figure 20 shows the streamlines and isotherms at various Rayleigh numbers for 0.243% concentration. This figure shows that with rise in Rayleigh number the flow intensity near walls increases as can also be clearly seen in figure 21. Moreover no change in streamline function along midline is observed near the centre of the cavity. Figure 21 shows the variation of streamline function ( $\psi$ ) along x direction at varied Rayleigh numbers for 0.243% magnetic nanofluid. A rise in the values of streamline function close to the wall and no variation for middle portion



**Figure 21.** Streamline function along Midline ( $Y=L/2$ ) of the cavity.

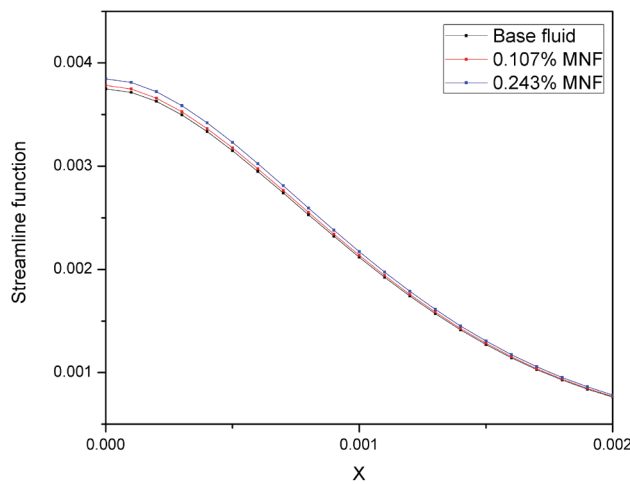


**Figure 22.** Variation of Streamline function with concentration close to wall (from  $X=0$  to  $X=0.02$ ).

of the cavity is seen. The increase in streamline function indicates increase in intensity of flow near the wall which in turn increases the heat transfer from the wall. The effect of nanoparticle addition is shown in figure 22 for Rayleigh number of  $10^7$ . Figure 22 shows a small enhancement in  $\Psi$  with rise in particle loading with maximum of 2.58% increase in  $\Psi$  for 0.243% concentration. The results demonstrate and exhibit the heat and flow enhancement characteristics of the nanofluids inside the cavity with Rayleigh number and concentration. In order to validate the results comparison is made with experimental results from the literature. As is seen from Figure 23 and 24 the results for Nusselt number are in close proximity with the results of Ho et al. [41] and Pattamatta et al. [42].

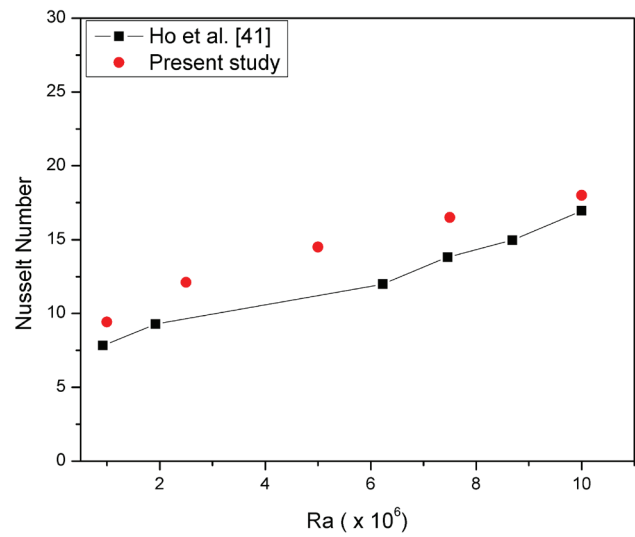


**Figure 23.** Validation of results of the present study for base fluid with experimental results from literature.

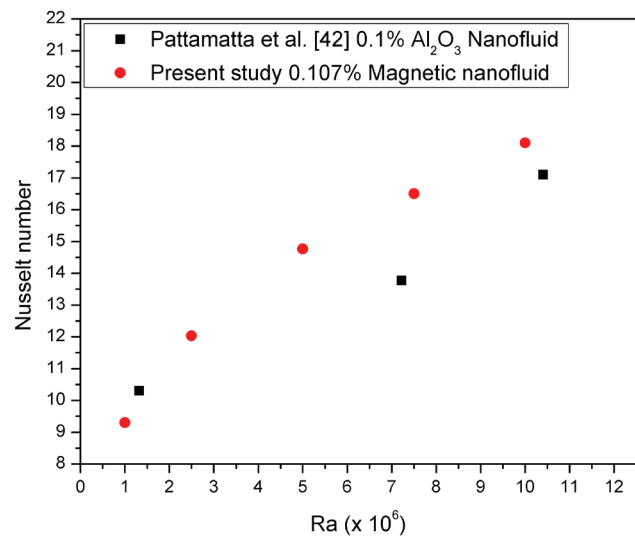


**Figure 24.** Validation of results of the present study for nanofluid with experimental results from literature.

## CONCLUSIONS

In this study, stable magnetic nanofluids have been synthesized for varied concentrations and their thermal and rheological properties have been investigated. It is concluded that:

- Thermal conductivity increases with the increase in the concentration of nanoparticles.
- Newtonian behavior is observed at low concentration and as the concentration increases the flow behavior changes to Non-Newtonian shear thinning. Thus, rheological behavior of nanofluids is dependent on shear rate as well as concentration.
- For all concentrations with rise in temperature the viscosity of nanofluids decreases and it increases with increase in concentration. An average viscosity enhancement of 8.2%, 18%, and 34.4% 40.2% is observed for 0.107%, 0.214%, 0.432% and 0.643% concentration respectively.
- Viscosity enhancement ratio is strongly dependent on concentration and is not significantly affected by temperature.
- The enhancement in viscosity is much more for ethylene glycol based  $\text{Fe}_3\text{O}_4$  nanofluids compared to enhancement in thermal conductivity.
- The ratio of enhancements in thermal conductivity and viscosity,  $E$  (K/V) is always below 1. Further it is observed that with rise in concentration there is a decrease in this ratio, thus limiting the applicability of magnetic nanofluids.
- Further from the simulation studies it is found that the use of magnetic nanofluid enhanced the heat transfer as is evident from increase in Nusselt number and heat transfer coefficient. This augmentation is strongly affected by the Rayleigh number.

## REFERENCES

- [1] Choi SUS. Enhancing thermal conductivity of fluids with nanoparticles. *ASME FED* 1995;231:99–105.
- [2] Masuda H, Ebata A, Teramae K, Hishinuma N. Alteration of thermal conductivity and viscosity of liquid by dispersing ultra-fine particles. *NetsuBussei* 1993;7:227–233. [\[CrossRef\]](#)
- [3] Eastman JA, Choi SUS, Li S, Yu W, Thompson LJ. Anomalously increased effective thermal conductivities of ethylene glycol-based nanofluids containing copper nanoparticles. *Appl Phys Lett* 2001;78:718–720. [\[CrossRef\]](#)
- [4] Choi SUS, Zhang ZG, Yu W, Lockwood FE, Grulke EA. Anomalous thermal conductivity enhancement in nanotube suspensions. *Appl Phys Lett* 2001;79:2252–2255. [\[CrossRef\]](#)
- [5] Das SK, Putta N, Thiesen P, Roetzel W. Temperature dependence of thermal conductivity enhancement for nanofluids. *J Heat Transf* 2003;125:567–574. [\[CrossRef\]](#)
- [6] Hwang YJ, Ahn YC, Shin HS, Lee CG, Kim GT, Park HS, Lee JK. Investigation on characteristics of thermal conductivity enhancement of nanofluids. *Curr Appl Phys* 2006;6(Suppl 6):1068–1071. [\[CrossRef\]](#)
- [7] Gulzar O, Qayoum A, Gupta R. Photo - thermal characteristics of hybrid nanofluids based on Therminol- 55 oil for concentrating solar collectors. *Appl Nanosci* 2018;9(20):1–11 [\[CrossRef\]](#)
- [8] Pourrajab R, Noghrehbadi A, Behbahani M, Hajidavalloo E. An efficient enhancement in thermal conductivity of water-based hybrid nanofluid containing MWCNTs-COOH and Ag nanoparticles: experimental study. *J Therm Anal Calorim* 2021;143:3331–3343. [\[CrossRef\]](#)
- [9] Yu W, Xie H, Chen L, Li Y. Enhancement of thermal conductivity of kerosene-based  $\text{Fe}_3\text{O}_4$  nanofluids prepared via phase-transfer method. *Colloids Surf A Physicochem Eng* 2010;355:109–113. [\[CrossRef\]](#)
- [10] Nkurikiyimfura I, Wang Y, Pan Z, Hu D. Enhancement of thermal conductivity of magnetic nanofluids in magnetic field. in *ICMREE2011 - Proceedings 2011 International Conference on Materials for Renewable Energy and Environment* 2011;2:1333–1337. [\[CrossRef\]](#)
- [11] Li Q, Xuan Y. Experimental investigation on heat transfer characteristics of magnetic fluid flow around a fine wire under the influence of an external magnetic field. *Exp Therm Fluid Sci* 2009;33:591–596. [\[CrossRef\]](#)
- [12] Parekh K, Lee HS. Magnetic field induced enhancement in thermal conductivity of magnetite nanofluid. *J Appl Phys* 2010;107:2–4. [\[CrossRef\]](#)
- [13] Philip J, Shima PD, Raj B. Enhancement of thermal conductivity in magnetite based nanofluid due to chainlike structures. *Appl Phys Lett* 2007;91:2005–2008. [\[CrossRef\]](#)
- [14] Gavili A, Zabihi F, Isfahani TD, Sabbaghzadeh J. The thermal conductivity of water base ferrofluids under magnetic field. *Exp Therm Fluid Sci* 2012;41:94–98. [\[CrossRef\]](#)
- [15] Li X, Zou C, Wang T, Lei X. Rheological behavior of ethylene glycol-based SiC nanofluids. *Int J Heat Mass Transf* 2015;84:925–930. [\[CrossRef\]](#)
- [16] Chen H, Ding Y, Tan C. Rheological behaviour of nanofluids. *New J Phys* 2007;9:367. [\[CrossRef\]](#)
- [17] Hong RY, Ren ZQ, Han YP, Li HZ, Zheng Y, Ding J. Rheological properties of water-based  $\text{Fe}_3\text{O}_4$  ferrofluids. *Chem Eng Sci* 2007;62:5912–5924. [\[CrossRef\]](#)
- [18] Pastoriza-Gallego MJ, Lugo L, Legido JL, Piñeiro MM. Rheological non-Newtonian behaviour of ethylene glycol-based  $\text{Fe}_2\text{O}_3$  nanofluids. *Nanoscale Res Lett* 2011;3:1–7. [\[CrossRef\]](#)
- [19] Ahmadi Nadooshan A, Eshgarf H, Afrand M. Measuring the viscosity of  $\text{Fe}_3\text{O}_4$ -MWCNTs/EG hybrid nanofluid for evaluation of thermal efficiency: Newtonian and non-Newtonian behavior. *J Mol Liq* 2018;253:169–177. [\[CrossRef\]](#)

- [20] Phuoc TX, Massoudi M. Experimental observations of the effects of shear rates and particle concentration on the viscosity of  $\text{Fe}_2\text{O}_3$ -deionized water nanofluids. *Int J Therm Sci* 2009;48:1294–1301. [CrossRef]
- [21] Anoop KB, Kabelac S, Sundararajan T, Das SK. Rheological and flow characteristics of nanofluids: Influence of electroviscous effects and particle agglomeration. *J Appl Phys* 2009;106:034909. [CrossRef]
- [22] Chen L, Xie H, Li Y, Yu W. Nanofluids containing carbon nanotubes treated by mechanochemical reaction. *Thermochim Acta* 2008;477:21–24. [CrossRef]
- [23] Syam Sundar L, Singh MK, Sousa ACM. Investigation of thermal conductivity and viscosity of  $\text{Fe}_3\text{O}_4$  nanofluid for heat transfer applications. *Int Commun Heat Mass Transf* 2013;44:7–14. [CrossRef]
- [24] Afrand M, Toghraie D, Ruhani B. Effects of temperature and nanoparticles concentration on rheological behavior of  $\text{Fe}_3\text{O}_4$ -Ag/EG hybrid nanofluid: An experimental study. *Exp Therm Fluid Sci* 2016;77:38–44. [CrossRef]
- [25] Kumar A, Subudhi S Preparation, characteristics, convection and applications of magnetic nanofluids: A review. *Heat Mass Transf* 2018;54:241–265. [CrossRef]
- [26] Platonic India Ltd. Graphene. Available at: <https://platonicnanotech.com/> Last Accessed Date: 25.09.2023.
- [27] DecagonDevices. Available at: <http://manuals.deca.com/Manuals> Last Accessed Date: 25.09.2023.
- [28] James Clerk M. A Treatise on Electricity and Magnetism. Cambridge: Cambridge University Press; 2010.
- [29] Xue QZ. Model for effective thermal conductivity of nanofluids. *Phys Lett A* 2003;307:313–317. [CrossRef]
- [30] Mints HA, Roy G, Nguyen CT, Doucet D. New temperature dependent thermal conductivity data for water-based nanofluids. *Int J Therm Sci* 2009;48:363–371. [CrossRef]
- [31] Timofeeva EV, Gavrilov AN, McCloskey JM, Tolmachev YV, Sprunt S, Lopatina LM, et al. Thermal conductivity and particle agglomeration in alumina nanofluids: Experiment and theory. *Phys Rev E* 2009;76:28–39. [CrossRef]
- [32] Sundar LS, Singh MK, Sousa ACM. Thermal conductivity of ethylene glycol and water mixture based  $\text{Fe}_3\text{O}_4$  nanofluid. *Int Commun Heat Mass Transf* 2013;49:17–24. [CrossRef]
- [33] Gulzar O, Qayoum A, Gupta R. Experimental study on stability and rheological behaviour of hybrid  $\text{Al}_2\text{O}_3$ - $\text{TiO}_2$  Therminol-55 nano fluids for concentrating solar collectors. 2019;352:436–444. [CrossRef]
- [34] Gulzar O, Qayoum A, Gupta R. Experimental study on thermal conductivity of mono and hybrid  $\text{Al}_2\text{O}_3$ - $\text{TiO}_2$  nanofluids for concentrating solar collectors. *Int J Energy Res* 2020;45:4370–4384. [CrossRef]
- [35] Krieger IM, Dougherty TJ. A mechanism for non-newtonian flow in suspensions of rigid spheres. *Trans Soc Rheol* 1959;3:137–152. [CrossRef]
- [36] Brinkman HC. The viscosity of concentrated suspensions and solutions. *J Chem Phys* 1952;20:571. [CrossRef]
- [37] Batchelor GK. The effect of Brownian motion on the bulk stress in a suspension of spherical particles. *J Fluid Mech* 1997;83:97–117. [CrossRef]
- [38] Einstein A. Investigations on the theory of Brownian motion. Furth R, (ed.). New York: Dover Publications; 1956.
- [39] De Vahl Davis G. Natural convection of air in a square cavity, a benchmark numerical solution. *Int J Numer Meth Fluids* 1984;3:249–264. [CrossRef]
- [40] Khanafer K, Vafai K, Lightstone M. Buoyancy-driven heat transfer enhancement in a two-dimensional enclosure utilizing nanofluids. *Int J Heat Mass Transf* 2003;46:3639–3653. [CrossRef]
- [41] Ho CJ, Liu WK, Chang YS, Lin CC. Natural convection heat transfer of alumina-water nanofluid in vertical square Enclosures: An experimental study. *Int J Therm Sci* 2010;49:1345–1353. [CrossRef]
- [42] Joshi PS, Pattamatta A. Buoyancy induced convective heat transfer in particle, tubular and flake type of nanoparticle suspensions. *Int J Therm Sci* 2017;122:1–11. [CrossRef]
- [43] Azeez K, Abu Talib AR, Ibraheem Ahmed R. Heat transfer enhancement for corrugated facing step channels using aluminium nitride nanofluid-numerical investigation. *J Therm Eng* 2022;8:734–747. [CrossRef]
- [44] Sereir T, Missoum A, Mebarki B, Elmir M, Douha M. Effect of the position of the hot source on mixed convection in a rectangular cavity. *J Therm Eng* 2022;8:538–550. [CrossRef]
- [45] Kilic M, Ullah A. Numerical investigation of effect of different parameter on heat transfer for a cross-flow heat exchanger by using nanofluids. *J Therm Eng* 2021;7(Suppl 14):1980–1989. [CrossRef]
- [46] Zahmatkesh I, Ardekani RA. Effect of magnetic field orientation on nanofluid free convection in a porous cavity: A heat visualization study. *J Therm Eng* 2020;6:170–186. [CrossRef]
- [47] Bayareh M, Nourbakhsh A. Numerical simulation and analysis of heat transfer for different geometries of corrugated tubes in a double pipe heat exchanger. *J Therm Eng* 2019;5:293–301. [CrossRef]
- [48] Madani K, Ben Maad R, Abidi-Saad A. Numerical Investigation of cooling a ribbed microchannel using nanofluid. *J Therm Eng* 2018;4:2408–2422. [CrossRef]
- [49] Kezzar M Nafir N, Tabet I, Khanetout A. A new analytical investigation of natural convection of non-newtonian nanofluids flow between two vertical flat plates by the generalized decomposition method (GDM). *J Therm Eng* 2018;4:2496–2508. [CrossRef]

- [50] Singh P, Sharma P, Gupta R, Wanchoo RK. Heat transfer characteristics of propylene glycol/water based magnesium oxide nanofluid flowing through straight tubes and helical coils. *J Therm Eng* 2018;4:1737–1755. [\[CrossRef\]](#)
- [51] Ahmed A, Qayoum A. Investigation on the thermal degradation, moisture absorption characteristics and antibacterial behavior of natural insulation materials. *Mater Renew Sustain Energy* 2021;10:1–10. [\[CrossRef\]](#)
- [52] Bashir M, Qayoum A, Saleem SS. Effect of banana peel powder on the fade and recovery of brake friction material. *JOM* 2022;74:2705–2715. [\[CrossRef\]](#)
- [53] Dilawar M, Qayoum A. Performance study of aluminium oxide based nanorefrigerant in an air-conditioning system. *Res Eng Struct Mater* 2023;9:147–162. [\[CrossRef\]](#)
- [54] Ali B, Qayoum A, Saleem S, Mir FQ. Synthesis and characterization of high-quality multi layered graphene by electrochemical exfoliation of graphite. *Res Eng Struct Mater* 2022;8:447–462. [\[CrossRef\]](#)
- [55] Qayoum A, Panigrahi P. Experimental investigation of heat transfer enhancement in a two-pass square duct by permeable ribs. *Heat Transf Eng* 2019;40:640–651. [\[CrossRef\]](#)
- [56] Bashir M, Qayoum A, Saleem SS. Experimental investigation of thermal and tribological characteristics of brake pad developed from eco-friendly materials. *J Bio-Tribo-Corrosion* 2021;7:1–13. [\[CrossRef\]](#)
- [57] Qayoum A, Panigrahi PK. Synthetic jet interaction with approaching turbulent boundary layer for heat transfer enhancement. *Heat Transf Eng* 2015;36:352–367. [\[CrossRef\]](#)
- [58] Ahmed A, Qayoum A, Mir FQ. Investigation of the thermal behavior of the natural insulation materials for low temperature regions. *J Build Eng* 2019;26:100849. [\[CrossRef\]](#)
- [59] Qayoum A, Gupta V, Panigrahi PK, Muralidhar K. Influence of Amplitude and Frequency Modulation on Flow Created by a Synthetic Jet Actuator. *Sens Actuators A Phys* 2010;162:36–50. [\[CrossRef\]](#)
- [60] Ahmed A, Qayoum A, Mir FQ. Spectroscopic studies of renewable insulation materials for energy saving in building sector. *J Build Eng* 2021;44:103300. [\[CrossRef\]](#)
- [61] Qayoum A, Gupta V, Panigrahi PK, Muralidhar K. Perturbation of a laminar boundary layer by a synthetic jet for heat transfer enhancement. *Int J Heat Mass Transf* 2010;53:5035–5057. [\[CrossRef\]](#)